

# Coupled interactions at the ionic graphene/water interface

Anton Robert,<sup>1,\*</sup> Hélène Berthoumieux,<sup>2,3,†</sup> and Marie-Laure Bocquet<sup>1,‡</sup>

<sup>1</sup>*PASTEUR, Département de chimie, École normale supérieure,*

*PSL University, Sorbonne Université, CNRS, 75005 Paris, France*

<sup>2</sup>*Sorbonne Université, CNRS, Laboratoire de Physique Théorique de la Matière Condensée (LPTMC, UMR 7600), F-75005 Paris, France*

<sup>3</sup>*Fachbereich Physik, Freie Universität Berlin, Arnimallee 14, Berlin, 14195, Germany*

We compute ionic free energy adsorption profiles at aqueous graphene interface by developing a self-consistent approach. To do so, we design a microscopic model for water and put the liquid on an equal footing with the graphene described by its electronic band structure. By evaluating progressively the electronic/dipolar coupled electrostatic interactions, we show that the coupling level including mutual graphene/water screening permits to recover remarkably the precision of extensive quantum simulations. We further derive the potential of mean force evolution of several alkali cations.

The peculiar properties of the water/graphene interface have been unveiled in pioneering experimental [1–3] and theoretical [4–9] studies. This results in particular in the extraordinary transport efficiency in water-filled carbon nanotubes and nanochannels [10–12]. Moreover, the presence of charges in the wet nanometric channels leads to exotic ionic behaviors [13–16] that are the cornerstone of energy storage applications [17] and blue energy harvesting [18]. Although experimental data [19, 20] regarding specific graphene-ion interactions in water are still few in numbers, the need to overtake classical molecular dynamics (MD) approximations and to model them at the same level as metal/liquid interfaces [21, 22] has been acknowledged. Beyond classical approaches, state-of-the-art quantum calculations combined with solvation codes [23–25] and even fully explicit ab initio methods [26, 27] – treating both the liquid and the solid at the Born-Oppenheimer level – represent the current state-of-the-art but their computational cost remains prohibitive for systematic investigations. On the other hand, recent semi-classical numerical studies have described graphene using a perfect metal [28], a Thomas-Fermi [29, 30], and an atomistic polarizable force field [21, 31] model. Nevertheless, these studies ignore the semimetallic band structure of graphene. Continuum electrostatic approaches [32, 33] permit to evaluate the well-known attractive “image-charge” electrostatic potential in a dielectric medium. Spatial correlations of both the fluid and the metal can *a priori* be included [34–36] to investigate microscopic effects. However, the self-consistent electrostatic problem is not yet addressed and collective interactions between electrons and molecules in the liquid are only partially and phenomenologically taken into account.

In this work, we develop a quantum/classical field framework to investigate electrostatic interactions at the aqueous graphene interface. We propose a microscopic model for the nonlocal dielectric properties of bulk and interfacial water and compute the polarization function of graphene from a tight-binding model. We evaluate the response function of a nanometric slab of water confined

between two graphene sheets by including gradually coupled electrostatic interactions between the electrons of the semimetal and the water molecules. This allows us to derive an accurate evolution of the potential of mean force (PMF) for a single cation solvated in the graphene channel. Finally we explore the as derived PMF profiles of a few alkali ions.

*Theoretical framework* Our framework, detailed in SI-Sec. 1, takes roots in quantum field theory, and uses Feynman diagrammatics to derive the Green’s function of the interfacial system. As predicted by quantum chemical calculations, the graphene/water interface presents a negligible electronic corrugation [5] and is chemically inactive with no mixing of electronic states [7, 37]. We focus on building the non-local linear response functions  $\chi$  of the system, that relates the mean induced charge density  $\langle n_{\text{ind}} \rangle$  to an external electrostatic potential  $\phi_{\text{ext}}$  generated by a charge distribution  $n_{\text{ext}}$ . The generic equations used to build the Green’s function  $w$  of the system and therefore the mean electrostatic potential  $\langle \phi_{\text{tot}} \rangle$  can be summarized as follows:

$$\begin{aligned} \phi_{\text{ext}} &= v * n_{\text{ext}} & \langle n_{\text{ind}} \rangle &= \chi * \phi_{\text{ext}} \\ w &= v + v * \chi * v & \langle \phi_{\text{tot}} \rangle &= w * n_{\text{ext}}, \end{aligned} \quad (1)$$

with  $v$  can denote the bare ( $v = 1/4\pi\epsilon_0 x$ , with  $x$  the distance in 3D space) or an effective Coulomb potential and  $*$  the spatial convolution. The starting assumption to build  $\chi$  is to consider that particles are independent and to derive an *non-interacting* response function  $\chi^{(0)}$ . Next,  $\chi^{(0)}$  is renormalized by considering interactions at the mean-field level: independent particles respond to the external potential plus the mean polarization potential  $\langle \phi_{\text{pol}} \rangle$  of the other similar particles. The induced charge density thus reads  $\langle n_{\text{ind}} \rangle = \chi^{(0)} * [\phi_{\text{ext}} + \langle \phi_{\text{pol}} \rangle]$  with  $\langle \phi_{\text{pol}} \rangle = v_{\text{inter}} * \langle n_{\text{ind}} \rangle$  and where  $v_{\text{inter}}$  is the effective interparticle potential. This recursive equation combined with Eq. 1 gives

$$\chi = \chi^{(0)} + \chi^{(0)} * v_{\text{inter}} * \chi. \quad (2)$$

Eq. 1 and Eq. 2 sets of equations give the definition for  $v_{\text{inter}}$  and are used in the following to build the response function of the water ( $\chi_w$ ) and the electronic ( $\chi_e$ ) part separately, but also to build  $\chi$  or  $w$  of the entire interfacial system. The interfacial system consists of a channel of nanometric height  $L$  made of two graphene sheets and filled with water.

**Water bulk** We now build the response function  $\chi_w$  of bulk water. Using Eq. 2, the effective electrostatic potential in bulk water  $v_{\text{inter}} = v_w^{\text{eff}}$  can be written  $v_w^{\text{eff}}(k) = 1/\chi_w^{(0)}(k) - 1/\chi(k)$ , with  $k = |\mathbf{k}|$ . The fluctuation-dissipation theorem gives  $\chi_w^{(0)}(k) = -\beta S_w^{(0)}(k)$  where  $\beta = 1/k_B T$  and  $S_w^{(0)}(k)$  is the single-molecule – or “self” – charge structure factor, and  $\chi_w(k) = -\beta S_w(k)$ ,  $S_w(k)$  the charge structure factor of the liquid. Here, we apply this framework to the widely-used 3 point-charge model of water, SPC/E [38]. The analytical expression of  $S_w^{(0)}(k)$  is given in SI-Sec.3.1.1.  $\chi(k)$  can be computed in a MD simulation – e.g. the results of [39] computing the polarization response function  $\bar{\chi}_w = -\chi_w(k)/\epsilon_0 k^2$  that are reported in Fig. 1a. The sharp peak of  $\bar{\chi}_w(k)$  centered at  $k \simeq 3 \text{ \AA}^{-1}$  illustrates the nonlocal and over-screening properties of water [40]. From the numerical knowledge of the effective Coulomb potential for water  $v_w^{\text{eff}}(k)$ , we suggest the following ansatz:

$$v_w^{\text{eff}}(k) = \frac{1}{\epsilon_0 \epsilon_w^{\text{eff}}} \left( \frac{1}{k^2} - \frac{1}{k^2 + \kappa^2} - \frac{\gamma e^{-k^2/2\kappa^2}}{\kappa^2 \sqrt{2\pi}} \right), \quad (3)$$

with the inverse screening length  $\kappa$ , the prefactor  $\gamma$  and the effective permittivity  $\epsilon_w^{\text{eff}}$  as parameters. The last one is fixed to recover the bulk dielectric permittivity of SPC/E water and can be expressed as a function of the molecular dipole moment and bulk density of the fluid. The values of  $(\kappa, \gamma)$  are adjusted to reproduce the position and the amplitude of the over-screening peak of  $\bar{\chi}_w$ . The ansatz ensures  $\chi_w(k) \rightarrow \chi_w^{(0)}(k)$  for  $k \rightarrow \infty$  (see details in SI-Sec. 3.1.2).

We plot the polarization response function derived from our framework,  $\bar{\chi}_w(k) = -(1/\chi_w^{(0)}(k) - v_w^{\text{eff}}(k))^{-1}/k^2 \epsilon_0$  (orange curve, Fig.1a). Our model captures nicely the dielectric properties of bulk water at low  $k$ .

**Water slab** We turn to the dielectric response of a water slab confined between two infinite flat interfaces in the  $(x,y)$  plane located in  $z=0$  and  $z=L$  respectively (see the sketch in Fig. 1b). We describe the system using cylindrical coordinates in real and Fourier spaces,  $\mathbf{x} = (\mathbf{r}, z)$  with  $\mathbf{r}$  lying in the interfacial plane and  $\mathbf{k} = (\mathbf{q}, q_z)$  with  $\mathbf{q}$  the in-plane Fourier component (see Fig. 1c right). According to the in-plane invariance, the response function can be written as  $\chi_w(q, z, z')$ . We show in SI-Sec. 3.2.1 that we can write

$$\chi_w^{(0)}(q, z, z') \simeq -\beta \frac{\sqrt{n_0(z)n_0(z')}}{n_0} S_w^{(0)}(q, |z - z'|) \quad (4)$$

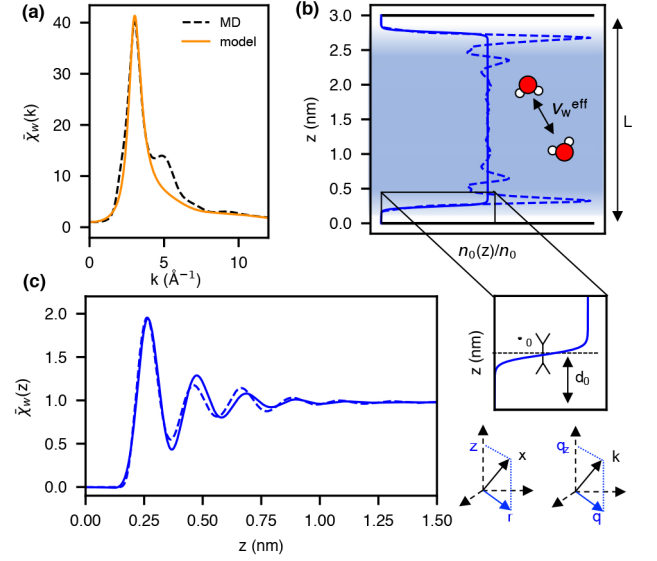


Figure 1. Dielectric response functions of water. (a) Susceptibility of SPC/E water obtained with MD [39] and with the theoretical model for  $(\epsilon_w^{\text{eff}} = 1.04)$  (see SI Sec.3.1.2),  $\kappa = 1.65 \text{ \AA}^{-1}$ ,  $\gamma = 0.99$ . We show the dimensionless quantities  $\bar{\chi}(k) = -\chi(k)/\epsilon_0 k^2$ . (b) Schematic drawing of the water slab and of the two considered molecular density profiles  $n_0(z)$  for  $L = 3 \text{ nm}$ . The inset shows the two parameters of the smoothed step function model for  $n_0(z)$ :  $d_0$  and  $\sigma_0$ . (c) Local dielectric susceptibility  $\bar{\chi}_w(z)$  of the slab  $P_z = \bar{\chi}_w(z)D_z$  corresponding to the molecular profile  $n_0(z)$ .

where  $S_w^{(0)}(q, |z - z'|) = \int \frac{dq_z}{2\pi} e^{iq_z|z - z'|} S_w^{(0)}(k)$  and  $n_0(z)$  is the molecular density profile that converges to bulk density  $n_0$  in the middle of the channel (see Fig. 1b). We assume that the water molecules interact in the slab between themselves as in bulk, so the slab-geometry effective potential  $v_w^{\text{eff}}(q, |z - z'|)$  can be obtained by Fourier transforming Eq. 3 (see SI-Sec. 3.2.2). To inverse Eq.2 and carry out all subsequent computations, we resort to matrix multiplications in the discretized space along  $z$  and  $z'$ . The  $(i, j)^{\text{th}}$  element of the matrix  $M[z_i, z'_j]$  is given by the function  $m(q, z_i, z'_j)$ . The solution of Eq. 2 reads  $X = (1 - X^{(0)} V_{\text{inter}}(dz)^2)^{-1} X^{(0)}$  where  $dz = 0.02 \text{ \AA}$  is the grid spacing and where a matrix of size  $[L/dz]^2$  has been inverted.

We now derive the local dielectric susceptibility  $\bar{\chi}_w(z)$ , relating the response polarization field  $P_z$  to a constant excitation  $\mathbf{D} = D_z \mathbf{e}_z$  such that  $P_z(z) = \bar{\chi}_w(z)D_z$ . We show in SI-Sec. 4.1 that

$$\bar{\chi}_w(z) = 1 - \frac{d}{dz} \left[ \int_0^L dz' \epsilon_w^{-1}(q \rightarrow 0, z, z') z' \right], \quad (5)$$

with  $w_w = \epsilon_w^{-1} * v = v + v * \chi_w * v$ ,  $w_w$  is the Green's function of the water slab alone, according to Eq. 1.

The slab water density profile  $n_0(z)$ , which describes the interaction between water and graphene, is an input of the model (see Eq. 4). We first consider a generic

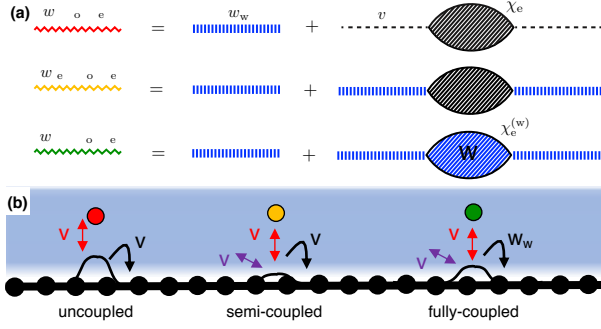


Figure 2. (a) Computed Feynman diagrams included in the Green's functions for various approximations. The colors of  $w$  match the one of curves in Fig. 3. The dashed line represents the Coulomb potential. The hatched bubble diagram depicts  $\chi_e$ . (b) Schematic illustration of the screening in the different cases (see text for interpretation).

smoothed step function model, which captures the vacuum layer between the fluid and a surface (encoded by  $d_0$ ) and the width ( $\sigma_0$ ) of the fluid interface (inset of Fig. 1b). In agreement with previous results [8, 41, 42], the susceptibility calculated in this framework (solid line in Fig. 1c) presents an alternation of over-responding ( $\bar{\chi}_w(z) > \chi_b$ ) and under-responding ( $\bar{\chi}_w(z) < \chi_b$ ) layers before reaching its bulk value  $\chi_b = 1 - 1/\epsilon_w$  for  $z > 1.25$  nm. Refining  $n_0(z)$  by extracting the hydrogen molecular density from a MD simulation [9] (see Fig. 1b) induces minor modifications in  $\bar{\chi}_w(z)$  (dotted line in Fig. 1c). This first result validates our analytical microscopic model for confined water.

*Graphene sheet* Regarding the solid phase, the non-interacting response function  $\chi_e^{(0)}$  can be computed and we choose a tight-binding model defined elsewhere [43]. Single-particle wavefunctions  $\psi_{\nu,\mathbf{p}}(\mathbf{x})$  and corresponding eigenenergies  $\epsilon_{\nu,\mathbf{p}}$  are labelled with the band index  $\nu$  and the in-plane wavevector  $\mathbf{p}$ . For one graphene sheet, assuming the small spatial extent of the  $p_z$  carbon orbitals, we consider the two-dimensional susceptibility  $\chi_e^{(0)}(q, z, z') = \chi_e^{(0)}(q)\delta(z)\delta(z')$  where  $\chi_e^{(0)}$  is (minus) the two-dimensional polarizability given by the bare bubble diagram [44]:

$$\chi_e^{(0)}(q) = \frac{2}{\mathcal{A}} \sum_{\nu,\mu,\mathbf{p}} |\lambda_{\mathbf{p},\mathbf{p}+\mathbf{q}}^{\nu,\mu}|^2 \frac{n_F(\epsilon_{\mu,\mathbf{p}+\mathbf{q}}) - n_F(\epsilon_{\nu,\mathbf{p}})}{\epsilon_{\mu,\mathbf{p}+\mathbf{q}} - \epsilon_{\nu,\mathbf{p}}}, \quad (6)$$

where  $\mathcal{A}$  is the surface area,  $n_F$  the Fermi-Dirac distribution and  $\lambda_{\mathbf{p},\mathbf{p}+\mathbf{q}}^{\nu,\mu} = \int d\mathbf{x} \psi_{\nu,\mathbf{p}}^*(\mathbf{x}) \psi_{\mu,\mathbf{p}+\mathbf{q}}(\mathbf{x}) e^{-i\mathbf{q}\cdot\mathbf{r}}$ . We compute Eq. 6 analytically at  $T = 0\text{K}$  [45] (see result in SI-Sec. 5.1) and use a Fermi level of  $E_F = k_B T$  to include a minimal number of free electrons. The response function  $\chi_e$  is built from Eq. 2 using the bare Coulomb

potential for the electron-electron interacting potential,  $v_{\text{inter}} = v$ , which corresponds to the well-known random-phase approximation [46] (see SI-Sec. 1.2). Case of two interacting graphene sheets are detailed in SI-Sec. 5.2.

*PMF modelling and coupled interactions* Turning to the computation of the PMF, we first derive the Coulomb energy at a mean field level defined as

$$F(z) = \frac{1}{2} \iint d\mathbf{x} d\mathbf{x}' n_{\text{ext}}(\mathbf{x}) \Delta w(\mathbf{x}, \mathbf{x}') n_{\text{ext}}(\mathbf{x}') \quad (7)$$

where  $\Delta w = w - v$ . A spherical test charge of radius  $b$  is placed in the channel at the altitude  $\mathbf{x} = (0, 0, z)$  such that  $n_{\text{ext}}(\mathbf{x}) = \pm e \delta(b - |\mathbf{x} - z\mathbf{e}_z|)/4\pi b^2$ . The test charge region is assumed to respond as water. We define the PMF as  $\Delta F(z) = F(z) - F(L/2)$ . It thus contains only electrostatic contributions and neglects the short-range Van der Waals interactions. We now gradually introduce coupled interactions in three steps labeled uncoupled, semi-coupled and fully-coupled to build  $w$  from the knowledge of  $\chi_e$  and  $\chi_w$ .

Fig. 2 reports the computed Feynman diagrams and the sketched coupling scenarios. First, we consider the uncoupled case, where water and graphene are blind to each other such that  $w$  is clearly separable:

$$w_{\text{uncoupled}} = w_w + v * \chi_e * v. \quad (8)$$

Secondly, we consider the semi-coupled scenario where the polarization charge on the graphene surface results from the potential exerted by the ion and surrounding water molecules. This is the sum of the bare ionic potential and the one induced by the solvating structure of dipoles, that is the screened potential that is obtained by the water slab Green's function  $w_w$  and therefore

$$w_{\text{semi-coupled}} = w_w + w_w * \chi_e * w_w. \quad (9)$$

It is equivalent to an interfacial semi-classical simulation adding a self-consistent optimization of the surface polarization at each time step, taking into account fixed – and equal to their values in vacuum – site-site interactions of the atomistic model of the metal. For analytical approaches, it corresponds to the ion-metal electrostatic interaction derived in the pioneering work of Kornyshev et al.[34] and later [47]. Finally, the last fully-coupled case unveils the presence of the polar liquid for electrons of the solid. Electron-electron interactions are effectively modified due to the presence of water, so that we introduce the in situ response function of the metal  $\chi_e^{(w)}$  which is built from Eq. 2 with  $v_{\text{inter}} = w_w$ . Note that this coupling effect can not be included in a simple way in the standard approaches [34, 47]. The most refined Green's function systems therefore reads

$$w_{\text{fully-coupled}} = w_w + w_w * \chi_e^{(w)} * w_w. \quad (10)$$

With the above  $w$  expressions, three different PMFs can be computed using Eq. 7. Note that the double inte-

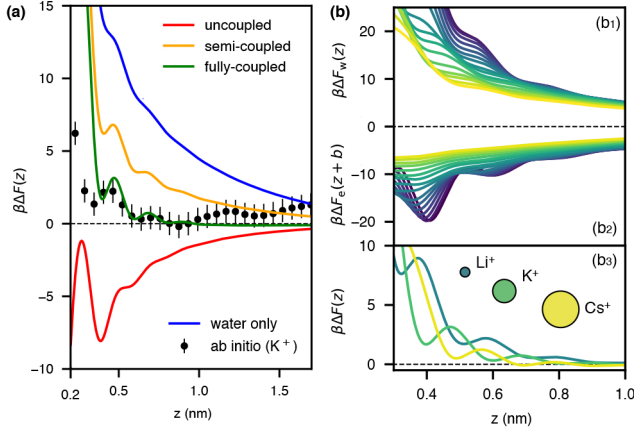


Figure 3. **(a)** PMF of  $K^+$  ( $b = 2 \text{ \AA}$ ) at the graphene-water interface. Models with increasing coupling (solid lines) compared to a graphene-free model (blue line) and ab initio simulations [27] (black dots with error bars). **(b)** Detailed contributions to the PMF from water ( $b_1$ ) and from graphene ( $b_2$ ) with increasing ionic radius from point charge (blue) to large radius (yellow). For  $\Delta F_e$ , the ionic center is placed at increasing altitude  $\mathbf{x} = (0, 0, z + b)$  for increasing radius. ( $b_3$ ) Comparative PMF for three alkali ions. The PMF for  $Li^+$  (resp.  $Cs^+$ ) is obtained using  $b = 1 \text{ \AA}$  (resp.  $b = 3 \text{ \AA}$ ).

gration of Eq. 7 is made in Fourier space and by matrix multiplication [48]. We compute all the PMFs for  $L = 6 \text{ nm}$  and using the first density model for  $n_0(z)$  with  $\sigma_0 = 0.3 \text{ \AA}$  [8]. The microscopic distance  $d_0$  is determined by imposing the long-wavelength limit of the surface charge structure factor of water at the interface [9] and equals  $d_0 = 1.3 \text{ \AA}$ .

To gain insights on the electronic and water contributions to the PMF, we decompose the free energy contribution into two terms:  $F = F_e + F_w$ , where  $F_w$  contains the contribution of water as in an air/water interface replacing  $w$  with  $w_w$  in Eq. 7. We could consider other substrates by changing  $\chi_e^{(0)}$  Eq. 6.

**Results & Discussions** Fig. 3a displays the resulting different computed profiles for  $\Delta F$  for one single positive charge of radius  $b = 2 \text{ \AA}$ , together with a reference curve computed recently from an ab initio molecular dynamics (AIMD) study, for  $K^+$  solvated in a 2nm thick water slab on graphene [27]. In the AIMD simulation the limited thickness of the water slab induces a second water/air interface explaining the non-monotonic and repulsive ab initio PMF behavior above 1nm. This large range of graphene-water distance ( $1 < z < 2 \text{ nm}$ ) is not meaningful here. Hence for sake of comparison, we shift the ab initio PMF such that it is vanishing in the middle of the water slab, for  $z$  around 1 nm (black dots, Fig. 3a). The water contribution  $\Delta F_w$  shows the expected repulsive behaviour of the ion at an air/interface (blue curve, Fig. 3a). Concerning the water/graphene interface, the uncoupled PMF profile (red curve, Fig. 3a) is strongly

attractive and presents oscillations with small amplitudes near the surface stemming from the non-local dielectric response of water. Moreover it deviates a lot from the ab initio plot.

Moving to the semi-coupled PMF profile (orange curve, Fig. 3a), its energy position is shifted to positive values fingerprinting a long-range repulsion and a net reduction of the graphene-ion interaction due to surrounding water molecules. Interestingly this result is in quantitative agreement with semi-classical simulations [21, 28, 49] using *ad hoc* surface polarization models (SI-Section 6.2). Finally the fully-coupled PMF curve (green curve in Fig. 3a) reveals a re-amplification of the wall-ion attraction by several thermal energy units and matches almost quantitatively the ab initio PMF. This is the key finding of our approach. The nice agreement suggests that this semi-analytical approach incorporating electrostatics in a self-consistent way, is able to reproduce some key features of the state-of-art reference PMF like the position and amplitude of the three local minima. The stabilizing effect present in the fully-coupled case can be qualitatively understood as follows. The absence of repulsive interaction between charge carriers would make them accumulate to one point in order to screen the ionic potential. Thanks to electron-electron interactions a finite polarization charge can accumulate on the surface as shown by the uncoupled case cartoon in Fig. 2b. Water molecules actually screen the ionic potential and reduce the polarization charge (semi-coupled case Fig. 2b), but in the last fully-coupled case, the presence of water effectively reduce electron-electron interactions - by roughly a factor of  $(\epsilon_w + 1)/2$  for electrons that are far apart as shown in SI-Sec. 6.3. As a result, the polarization charge gets re-amplified and so does the surface-ion screened potential. The plots differ significantly at short distance,  $z < 0.5 \text{ nm}$ , where non-electrostatic contributions of the PFM - not considered here - are dominant [33].

We now investigate the variations of the PMF with varying radius  $b$  ranging from point charge to  $3 \text{ \AA}$  with detailed contributions from water and graphene. Fig. 3b1 shows that water repels more strongly smaller ions from the interface. This can be understood by considering the hydrated radius of the cations - defined in continuous theories as the range on which the ion polarizes the surrounding fluid - that is inversely proportional to the ionic radius [50]. Coming from the bulk,  $Li^+$  is the first to break its solvation shell. Fig. 3b2 compares the non-monotonic surface contribution  $\Delta F_e$  for the series of ions, which center is shifted so that the available space for water molecules between ion and surface is equal for each ion. We link the increasing attraction for smaller radii to the ordering degree of the hydration shells as follows. In the limit of poorly structured hydration shells - e.g. for  $Cs^+$  - we find the monotonic surface-ion potential of an attenuated charge in vacuum. The opposite limit is a point charge with three highly ordered hydration shells.



This gives rise to three special places where ice-like water, with a low permittivity, is practically transparent to the potential stemming from the polarization charge on the graphene surface. Summing both contributions in Fig. 3b<sub>3</sub> for three cations in the alkali series leads to complex PMF profiles. We observe that for increasing radius the three local minima are stabilized in energy in agreement with an increased capacitance [20] and a reduced hydration energy [24]. Indeed small ions like Li<sup>+</sup> manifest a strong solvation environment difficult to break hampering its adsorption. Proceeding down the series, Cs<sup>+</sup> yields a weak solvation shell which can be easily desolvated at the graphene interface.

**Conclusion** In this letter, we build a self-consistent theoretical framework which permits to investigate analytically the single ionic adsorption at the graphene/water interface. By including the semimetallic band structure of graphene, building a microscopic model for interfacial water and considering the mutual screening of the two materials, we obtained results that are in excellent agreement with expensive quantum free energy perturbation methods, at a negligible computational cost. Our PMF predictions for the alkali series are in agreement with experimental observations and permit to distinguish the liquid water and graphene surface contributions. We hope that this versatile and generalizable method, will renew some interest in semi-analytical approaches and be used to investigate more complex systems involving for example ion-ion interactions in nanochannels.

**Acknowledgments** A.R. thanks D. Borgis for discussions. A.R. and M.-L.B. acknowledge funding from EU H2020 Framework Programme/ERC Advanced Grant agreement number 785911-Shadoks. H. B. acknowledges funding from Humboldt Research Fellowship Programme for Experienced Researchers.

## CODE AVAILABILITY

Our code is freely available in the GitHub repository [https://github.com/anton-smirnov-robert/pmf\\_water\\_graphene](https://github.com/anton-smirnov-robert/pmf_water_graphene).

---

\* [anton.robert@ens.fr](mailto:anton.robert@ens.fr)

† [helene.berthoumieux@sorbonne-universite.fr](mailto:helene.berthoumieux@sorbonne-universite.fr)

‡ [marie-laure.bocquet@ens.fr](mailto:marie-laure.bocquet@ens.fr)

- [1] B. Radha, A. Esfandiar, F. C. Wang, A. P. Rooney, K. Gopinadhan, A. Keerthi, A. Mishchenko, A. Janardanan, P. Blake, L. Fumagalli, M. Lozada-Hidalgo, S. Garaj, S. J. Haigh, I. V. Grigorieva, H. A. Wu, and A. K. Geim, *Nature* **538**, 222 (2016).
- [2] E. Secchi, S. Marbach, A. Niguès, D. Stein, A. Siria, and L. Bocquet, *Nature* **537**, 210 (2016).
- [3] L. Fumagalli, A. Esfandiar, R. Fabregas, S. Hu, P. Ares, A. Janardanan, Q. Yang, B. Radha, T. Taniguchi, K. Watanabe, G. Gomila, K. S. Novoselov, and A. K. Geim, *Science* **360**, 1339 (2018).
- [4] Y. Wu and N. R. Aluru, *The Journal of Physical Chemistry B* **117**, 8802 (2013).
- [5] G. Tocci, L. Joly, and A. Michaelides, *Nano Letters* **14**, 6872 (2014).
- [6] R. P. Misra and D. Blankschtein, *The Journal of Physical Chemistry C* **121**, 28166 (2017).
- [7] J. G. Brandenburg, A. Zen, M. Fitzner, B. Ramberger, G. Kresse, T. Tsatsoulis, A. Grüneis, A. Michaelides, and D. Alfè, *The Journal of Physical Chemistry Letters*, 358 (2019).
- [8] G. Monet, F. Bresme, A. Kornyshev, and H. Berthoumieux, *Physical Review Letters* **126**, 216001 (2021).
- [9] N. Kavokine, M.-L. Bocquet, and L. Bocquet, *Nature* **602**, 84 (2022).
- [10] S. Faucher, N. Aluru, M. Z. Bazant, D. Blankschtein, A. H. Brozena, J. Cumings, J. Pedro de Souza, M. Elimlech, R. Epsztein, J. T. Fourkas, A. G. Rajan, H. J. Kulik, A. Levy, A. Majumdar, C. Martin, M. McEldrew, R. P. Misra, A. Noy, T. A. Pham, M. Reed, E. Schwelger, Z. Siwy, Y. Wang, and M. Strano, *The Journal of Physical Chemistry C* **123**, 21309 (2019).
- [11] L. Bocquet, *Nature Materials* **19**, 254 (2020).
- [12] N. Kavokine, R. R. Netz, and L. Bocquet, *Annual Review of Fluid Mechanics* **53**, 377 (2021).
- [13] A. Siria, P. Poncharal, A.-L. Biance, R. Fulcrand, X. Blase, S. T. Purcell, and L. Bocquet, *Nature* **494**, 455 (2013).
- [14] A. Esfandiar, B. Radha, F. C. Wang, Q. Yang, S. Hu, S. Garaj, R. R. Nair, A. K. Geim, and K. Gopinadhan, *Science* **358**, 511 (2017).
- [15] J. Comtet, A. Niguès, V. Kaiser, B. Coasne, L. Bocquet, and A. Siria, *Nature Materials* **16**, 634 (2017).
- [16] T. Mouterde, A. Keerthi, A. R. Poggoli, S. A. Dar, A. Siria, A. K. Geim, L. Bocquet, and B. Radha, *Nature* **567**, 87 (2019).
- [17] M. Salanne, B. Rotenberg, K. Naoi, K. Kaneko, P.-L. Taberna, C. P. Grey, B. Dunn, and P. Simon, *Nature Energy* **1**, 16070 (2016).
- [18] A. Siria, M.-L. Bocquet, and L. Bocquet, *Nature Reviews Chemistry* **1**, 0091 (2017).
- [19] D. L. McCaffrey, S. C. Nguyen, S. J. Cox, H. Weller, A. P. Alivisatos, P. L. Geissler, and R. J. Saykally, *Proceedings of the National Academy of Sciences* **114**, 13369 (2017).
- [20] P. Iamprasertkun, W. Hirunpinyopas, A. Keerthi, B. Wang, B. Radha, M. A. Bissett, and R. A. W. Dryfe, *The Journal of Physical Chemistry Letters* **10**, 617 (2019).
- [21] R. P. Misra and D. Blankschtein, *The Journal of Physical Chemistry C* **125**, 2666 (2021).
- [22] L. Scalfi, M. Salanne, and B. Rotenberg, *Annual Review of Physical Chemistry* **72**, 189 (2021).
- [23] C. D. Williams, J. Dix, A. Troisi, and P. Carbone, *The Journal of Physical Chemistry Letters* **8**, 703 (2017).
- [24] C. Zhan, M. R. Ceron, S. A. Hawks, M. Otani, B. C. Wood, T. A. Pham, M. Stadermann, and P. G. Campbell, *Nature Communications* **10**, 4858 (2019).
- [25] M. Ruggeri, K. Reeves, T.-Y. Hsu, G. Jeanmairet, M. Salanne, and C. Pierleoni, *The Journal of Chemical Physics* **156**, 094709 (2022).

- [26] B. Grosjean, M.-L. Bocquet, and R. Vuilleumier, *Nature Communications* **10**, 1656 (2019).
- [27] L. Joly, R. H. Meißner, M. Iannuzzi, and G. Tocci, *ACS Nano* **15**, 15249 (2021).
- [28] C. Y. Son and Z.-G. Wang, *Proceedings of the National Academy of Sciences* **118**, e2020615118 (2021).
- [29] L. Scalfi, T. Dufils, K. G. Reeves, B. Rotenberg, and M. Salanne, *The Journal of Chemical Physics* **153**, 174704 (2020).
- [30] A. Schlaich, D. Jin, L. Bocquet, and B. Coasne, *Nature Materials* **21**, 237 (2022).
- [31] R. P. Misra and D. Blankschtein, *Langmuir* **37**, 722 (2021).
- [32] J. Schwinger, in *Classical Electrodynamics* (Westview Press, 1998).
- [33] P. Loche, C. Ayaz, A. Schlaich, D. J. Bonthuis, and R. R. Netz, *The Journal of Physical Chemistry Letters* **9**, 6463 (2018).
- [34] M. A. Vorotyntsev and A. A. Kornyshev, *Zh. Eksp. Teor. Fiz.* **72**, 1008 (1980).
- [35] A. A. Kornyshev and M. A. Vorotyntsev, *Surface Science* **101**, 23 (1980).
- [36] A. M. Gabovich, M. S. Li, H. Szymczak, and A. I. Voitenko, *Surface Science* **606**, 510 (2012).
- [37] X. Li, J. Feng, E. Wang, S. Meng, J. Klimeš, and A. Michaelides, *Physical Review B* **85**, 085425 (2012).
- [38] H. J. C. Berendsen, J. R. Grigera, and T. P. Straatsma, *The Journal of Physical Chemistry* **91**, 6269 (1987).
- [39] G. Jeanmairet, N. Levy, M. Levesque, and D. Borgis, *Journal of Physics: Condensed Matter* **28**, 244005 (2016).
- [40] P. A. Bopp, A. A. Kornyshev, and G. Sutmann, *Physical Review Letters* **76**, 1280 (1996).
- [41] J.-P. Hansen and I. R. McDonald, *Theory of simple liquids* (Academic Press, 2013).
- [42] D. J. Bonthuis, S. Gekle, and R. R. Netz, *Langmuir* **28**, 7679 (2012).
- [43] A. H. Castro Neto, F. Guinea, N. M. R. Peres, K. S. Novoselov, and A. K. Geim, *Reviews of Modern Physics* **81**, 109 (2009).
- [44] G. D. Mahan, *Many-Particle Physics* (Springer US, 1990).
- [45] E. H. Hwang and S. Das Sarma, *Physical Review B* **75**, 205418 (2007).
- [46] D. Bohm and D. Pines, *Physical Review* **92**, 609 (1953).
- [47] V. Kaiser, J. Comtet, A. Niguès, A. Siria, B. Coasne, and L. Bocquet, *Faraday Discussions* **199**, 129 (2017).
- [48] Using  $N_{\text{ext}}[z] = J_0(q\sqrt{b^2 + (z - z_0)^2})/2b$  with  $J_0$  being the zeroth order Bessel function, we compute  $F(z_0) = \frac{1}{2} \int_0^{+\infty} \frac{dq}{2\pi} q \left[ N_{\text{ext}}^\dagger(W - V)N_{\text{ext}} \right](q)$ , for the three Green's functions, in log-log space using  $q = e^y E_F/v_F$ ,  $y \in [-1, 8]$  and  $N_y = 100$  for convergence. Note that  $V[z, z'] = e^{-q|z-z'|}/2\epsilon_0 q$ .
- [49] L. Scalfi and B. Rotenberg, *Proceedings of the National Academy of Sciences* **118**, e2108769118 (2021).
- [50] Y. Marcus, *Chemical Reviews* **109**, 1346 (2009).

# Coupled interactions at the ionic graphene/water interface

Anton Robert, Hélène Berthoumieux and Marie-Laure Bocquet

January 9, 2023

# Contents

<b>1</b>	<b>Building dielectric response functions</b>	<b>2</b>
1.1	Response functions . . . . .	2
1.2	Mean field correction: From $\chi^{(0)}$ to $\chi$ . . . . .	2
<b>2</b>	<b>The metal-like/liquid interface</b>	<b>3</b>
2.1	Hamiltonian of the system . . . . .	3
2.2	Response function at the interface . . . . .	5
2.3	Special case of the slit geometry . . . . .	6
<b>3</b>	<b>Water model</b>	<b>6</b>
3.1	Bulk water . . . . .	6
3.1.1	Non-interacting susceptibility $\chi_w^{(0)}(k)$ . . . . .	6
3.1.2	Effective potential $v_w^{\text{eff}}(k)$ . . . . .	8
3.2	Interfacial water . . . . .	9
3.2.1	Non-interacting susceptibility $\chi_w^{(0)}(q, z, z')$ . . . . .	9
3.2.2	Effective potential $v_w^{\text{eff}}(q,  z - z' )$ . . . . .	10
3.2.3	Matrix filling . . . . .	10
<b>4</b>	<b>Local dielectric susceptibility <math>\bar{\chi}_w(z)</math></b>	<b>10</b>
4.1	Expression from $\chi_w(q, z, z')$ . . . . .	10
4.2	Comparison with Landau-Ginzburg model . . . . .	11
<b>5</b>	<b>Graphene model</b>	<b>11</b>
5.1	The non-interacting susceptibility $\chi_e^{(0)}(q, z, z')$ . . . . .	11
5.2	The interacting susceptibility $\chi_e^{(w)}(q, z, z')$ . . . . .	12
<b>6</b>	<b>Supplementary discussions</b>	<b>13</b>
6.1	Long-wavelength limit error for water . . . . .	13
6.2	Comparison with other studies considering a metallic behavior of the surface . . . . .	13
6.3	Electron-electron potential attenuation . . . . .	13

## Notations

Throughout those notes, the Fourier transform is defined as follows :

$$f(\mathbf{k}) = \int d^3\mathbf{x} f(\mathbf{x}) e^{-i\mathbf{k}\mathbf{x}} \quad f(\mathbf{x}) = \int \frac{d^3\mathbf{k}}{(2\pi)^3} f(\mathbf{k}) e^{i\mathbf{k}\mathbf{x}}$$

We use cylindrical coordinates in real  $\mathbf{x} = (\mathbf{r}, z)$  and reciprocal space  $\mathbf{k} = (\mathbf{q}, q_z)$ .

# 1 Building dielectric response functions

## 1.1 Response functions

We consider a thermodynamically closed system such that the term external refers to something that is not a part of the physical system under scrutiny. Under the application of a perturbing external electrostatic potential  $\phi_{\text{ext}}(\mathbf{x}, t)$ , it responds by generating a charge density deviance  $n_{\text{ind}}(\mathbf{x}, t)$  - therefore induced by the latter. We will focus on the statistically averaged - denoted  $\langle \cdot \rangle$  - deviation produced by the system, in space-time - denoted for short by  $1 \equiv (\mathbf{x}_1, t_1)$ . Note that Linear response theory relates both quantities via the response function - or susceptibility -  $\chi$  as follows

$$\langle n_{\text{ind}}(1) \rangle = \int d2 \chi(1, 2) \phi_{\text{ext}}(2). \quad (1)$$

The total charge density of the system  $n = n_0 + n_{\text{ind}}$  might not be equal to  $n_{\text{ind}}$  if, without the external perturbation, an inhomogeneity is already present in the system. In turn, the averaged charge density deviance creates an averaged induced electrostatic potential  $\phi_{\text{ind}}$  that can be written

$$\langle \phi_{\text{ind}}(1) \rangle = \int d2 v(1, 2) \langle n_{\text{ind}}(2) \rangle. \quad (2)$$

Here we have used the *Green's function method* (Schwinger, 1998) to solve Poisson's equation so that the kernel is the Coulomb interaction between two particles of elementary charge (we use  $e = 1$ ) in vacuum that reads

$$v(1, 2) = \frac{1}{4\pi\epsilon_0} \frac{\delta(t_1 - t_2)}{|\mathbf{x}_1 - \mathbf{x}_2|}, \quad (3)$$

where  $\epsilon_0$  is the dielectric permittivity of vacuum. Accordingly, we write Eq. 2 for the external potential  $\phi_{\text{ext}}$  that arises from an external charge density  $n_{\text{ext}}$ . The statistically averaged total potential in the system is given by  $\langle \phi_{\text{tot}} \rangle = \langle \phi_{\text{ext}} \rangle + \langle \phi_{\text{ind}} \rangle$ . Combining Eq. 1 and Eq. 2 we can write the Green's function of the system  $w(1, 2)$  as

$$w(1, 1') = v(1, 1') + \iint d2 d3 v(1, 2) \chi(2, 3) v(3, 1'). \quad (4)$$

The linearity of Poisson's equation makes the introduction of  $w$  helpful because the total potential then reads

$$\langle \phi_{\text{tot}}(1) \rangle = \int d1' w(1, 1') n_{\text{ext}}(1'). \quad (5)$$

Those last equations directly establish the link between the averaged total potential  $\langle \phi_{\text{tot}} \rangle$  in the system and  $\chi$ , its two-point susceptibility. Regarding the general structure of  $w$  in Eq. 4, it is constituted of two objects linked by convolutions. To prepare future complexifications, we represent by a diagram the bare potential  $v$  and  $\chi$ .

$$1 \cdots \cdots 2 = v(1, 2) \quad 1 \text{---} \text{---} \text{---} 2 = \chi(1, 2) \quad (6)$$

We define that their link represents a convolution in space-time. Therefore, we can represent the Green's function as follows

$$w(1, 1') = 1 \cdots \cdots 1' + 1 \cdots \cdots \text{---} \text{---} \text{---} \cdots \cdots 1'. \quad (7)$$

## 1.2 Mean field correction: From $\chi^{(0)}$ to $\chi$ .

To build the response function  $\chi$  of a system containing indistinguishable particles, we start from the simplest possible version and enrich the description from it. The first - drastic - physical assumption is to consider that the particles are *independent* so that we first construct the *non-interacting* response function  $\chi^{(0)}$  using a microscopic model.

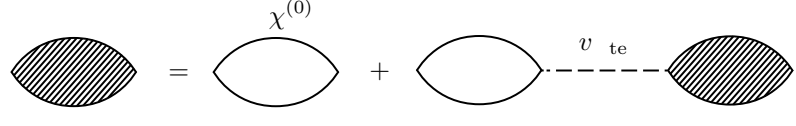
Enriching the description of the system requires considering interparticle interactions. In this work we use a mean field method. Be it for electrons in a metal (Mahan, 1990) or in simple liquids (Hansen and McDonald,



2013), the mean field method is a well-known renormalization scheme for homogeneous media to take into account the collective behavior of particles. It amounts to considering that independent particles respond to the external potential  $\phi_{\text{ext}}$  plus the *mean* polarization potential  $\langle\phi_{\text{pol}}\rangle = v_{\text{inter}} * \langle n_{\text{ind}}\rangle$  of the other similar particles - here  $v_{\text{inter}}$  is the interparticle potential and  $*$  denotes the space-time convolution. In other words, the mean induced charge density is given by the sum of the two contributions that reads

$$\langle n_{\text{ind}}(1)\rangle = \int d2\chi^{(0)}(12) \left[ \phi_{\text{ext}}(2) + \int d3v_{\text{inter}}(23)\langle n_{\text{ind}}(3)\rangle \right]. \quad (8)$$

The recursive nature of this interparticle *renormalization scheme* is captured by the integral equation for the response function  $\chi$  which reads

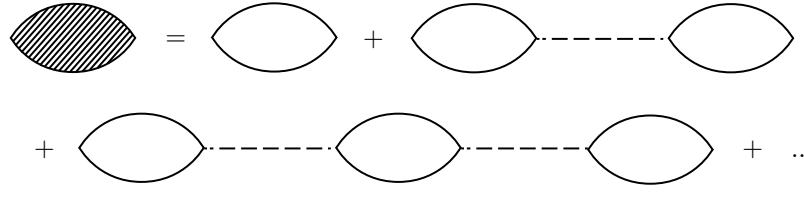


$$\text{hatched bubble} = \text{bare bubble} + \text{bare bubble} \cdots \text{dashed line } v_{te} \cdots \text{hatched bubble}, \quad (9)$$

or in equation

$$\chi(11') = \chi^{(0)}(11') + \iint d2d3\chi^{(0)}(12)v_{\text{inter}}(23)\chi(31'). \quad (10)$$

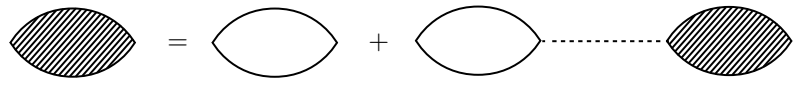
Note that the introduction of  $\chi$  is a short-cut notation for an infinite number of convolutions between  $\chi^{(0)}$  and  $v_{\text{inter}}$ , that are the elementary bricks. Indeed, by writing the beginning of the infinite sum



$$\text{hatched bubble} = \text{bare bubble} + \text{bare bubble} \cdots \text{dashed line} \cdots \text{bare bubble} + \text{bare bubble} \cdots \text{dashed line} \cdots \text{bare bubble} \cdots \text{dashed line} \cdots \text{bare bubble} + \dots, \quad (11)$$

we can observe that we have actually re-organized or *renormalized* an infinite sum of diagrams involving only  $\chi^{(0)}$  and  $v_{\text{inter}}$ . Turning to the topographic structure of  $w$  when the diagram depicted by  $\chi$  is decomposed, it consists in enumerating all diagrams that can be build with  $\chi^{(0)}$  and  $v_{\text{inter}}$ , that start and end with a Coulomb leg.

A special important case of mean-field renormalization is the random phase approximation (RPA) (Bohm and Pines, 1953). It is equivalent to identifying the interparticle mean-field potential with the direct potential - e.g.  $v_{\text{inter}} = v$  for classical point charges. For electrons, in the RPA, the potential can also include an exchange-correlation potential, but those refinements are left out of this study. We attribute the *bare bubble* diagram to  $\chi_e^{(0)}$  and the *hatched bubble* diagram to the RPA response function for electrons that we denote  $\chi_e$  that reads



$$\text{hatched bubble} = \text{bare bubble} + \text{bare bubble} \cdots \text{dashed line} \cdots \text{hatched bubble}. \quad (12)$$

## 2 The metal-like/liquid interface

### 2.1 Hamiltonian of the system

In the framework of quantum field theory, we will use a bosonic operator to depict the charge density of each medium  $\hat{n}(\mathbf{x}, t)$ , with  $\mathbf{x} = (\mathbf{r}, z)$  and  $n = \langle\hat{n}\rangle$  is the corresponding expectation value. It can either depicts the fictitious charge density operator of the classical Gaussian liquid  $\hat{n}_w$  Kavokine *et al.* (2022) or the nuclear charge density operator of the solid lattice  $\hat{n}_n$ . The creation and annihilation Fermi fields that describe the behavior of the electrons will be denoted  $\Psi^\dagger(\mathbf{x}, t)$  and  $\Psi(\mathbf{x}, t)$  such that the electronic charge density can be written  $\hat{n}_e(\mathbf{x}, t) = \Psi^\dagger(\mathbf{x}, t)\Psi(\mathbf{x}, t)$ . We consider the Coulomb interaction between partial atomic charges on classical molecules in the liquid, electrons and nuclei in the solid. The Hamiltonian of the system can be written  $H = H_0 + H_{\text{int}}$  with the quadratic Hamiltonian  $H_0 = H_w^{(0)} + H_e^{(0)} + H_n^{(0)}$ , for the electrons, liquid molecules and nuclei respectively that contains one-particle terms only.

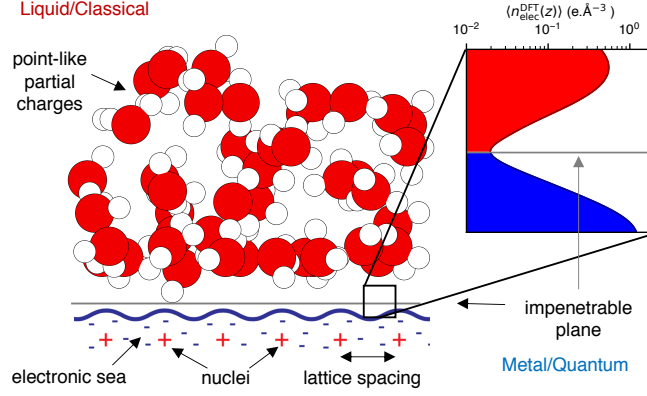


Figure 1: Schematic drawing of the metal/liquid interface. The zoom shows the behavior of the total electronic density near the interface between graphene and water. It is obtained with a static DFT calculation on a *ab initio* snapshot.

The crystal lattice, made of positively charged nuclei cannot be stable without considering an implicit interaction with the electrons that makes forces between nuclei nearly harmonic and not purely repulsive. In turn, the eigenstates of the electrons differ from the ones of the free electron gas because they feel the potential produced by the clamp nuclei. Herein, we will be interested in time-averaged quantities so that nuclei, with their core electrons, can be considered to be fixed on their equilibrium positions. As a result, they do not participate in the polarization charge and can be removed from the description by considering an appropriate tight-binding model that takes into account the lattice for valence electrons so that  $H_0 = H_w^{(0)} + H_e^{(n)}$ . Ignoring exchange and correlation interactions between electrons, we read

$$H_{\text{int}} = U_{ee} + U_{ew} + U_{ww}, \quad (13)$$

where the electronic interactions  $U_{ee}$  have to be explicitated with the Fermi fields to remove the diverging self-energy term - i.e.

$$U_{ee} = \frac{1}{2} \iint d1d2 \Psi^\dagger(1) \Psi^\dagger(2) v(1,2) \Psi(1) \Psi(2), \quad (14)$$

but where the other interactions can be clearly expressed in a more intuitive two-body form:

$$U_{ew} = \iint d1d2 \hat{n}_e(1) v(1,2) \hat{n}_w(2), \quad (15)$$

$$U_{ww} = \frac{1}{2} \iint d1d2 \hat{n}_w(1) v_w^{\text{eff}}(12) \hat{n}_w(2) \quad (16)$$

**Liquid part** For the liquid, the expression of  $v_w^{\text{eff}}$  is unknown. Nevertheless, by switching off the charge of electrons, we can isolate the excess term  $U_{ww}$  as follows:

$$U_{ww} = H - H_w^{(0)}.$$

The remaining Gaussian classical field is defined by its correlation function so that those Hamiltonians can be written in the form of

$$H[n_w] = - \iint d1d2 n_w(1) \chi_w^{-1}(12) n_w(2) \quad (17)$$

$$H_w^{(0)}[n_w] = - \iint d1d2 n_w(1) [\chi_w^{(0)}]^{-1}(12) n_w(2) \quad (18)$$

Note that  $\chi_w$  is the response function of the liquid slab alone and  $\chi_w^{(0)}$  is the *ideal* or *non-interacting* response function of the liquid slab. Consequently, we can write a general expression for  $v_w^{\text{eff}}$  using Eq. 16, 17, 18 that reads

$$v_{\mathbf{w}}^{\text{eff}}(12) = \left[ \chi_{\mathbf{w}}^{(0)} \right]^{-1} (12) - \chi_{\mathbf{w}}^{-1}(12). \quad (19)$$

Inserting Eq.19 in the mean field renormalization equation Eq.10, we understand that it is satisfied for  $v_{\text{inter}} = v_{\text{w}}^{\text{eff}}$  so that  $v_{\text{w}}^{\text{eff}}$  is the *charge-charge mean field potential in water*. This prompts us to introduce a diagram for the response function of the liquid. We have used the precedent diagrams for electrons and we therefore introduce a new white and hatched ball-and-stick representation for  $\chi_{\text{w}}^{(0)}$  and  $\chi_{\text{w}}$  respectively. The mean field equation Eq. 9, for the case of a water slab alone reads

$$\text{Diagram 1} = \text{Diagram 2} + \text{Diagram 3} \quad (20)$$

## 2.2 Response function at the interface

From the previous sections, we have guessed some rules for constructing diagrams that would lead to the Green's function of the system:

- (i) Draw all possible *linked* diagrams with  $\chi_w^{(0)}$  and  $\chi_e^{(0)}$  that start and ends with a Coulomb leg  $v$ . The links are given by the mean-field potential between particles.
- (ii) *Re-sum* the diagrams to make *renormalized* response functions appear.
- (iii) Write down the equation by reading the diagrams: a link represents a *convolution* in space-time.

Those rules stem from Feynman ones and are adapted to our case in which we focus on response functions. They lead to a result that can be derived with the functional formulation of quantum field theory (Hedin and Lundqvist, 1970; Giustino, 2017).

We re-organize all possible linked diagrams as prescribed by the aforementioned rules. There are 2 ways of re-summing the diagrams to put forward either electrons or water molecules. We chose to separate the contribution of the liquid alone. The Green's function of the liquid slab alone reads

$$w_w = \text{diagram 1} + \text{diagram 2} \quad (21)$$

The response function of electrons  $\chi_e^{(0)}$  can now be renormalized at the mean field level that we have seen in Eq. 10, except that electrons interact via the Coulomb potential screened by water so that  $v_{\text{inter}} = w_w$ . This means that we need to introduce the *in situ* response function of electrons  $\chi_e^{(w)}$  that reads

$$\chi_e^{(w)} = \text{diagram of a lens with label } W \text{ inside} = \text{diagram of an empty lens} + \text{diagram of an empty lens connected to a lens with label } W \text{ inside by a vertical dashed line} . \quad (22)$$

Finally, all diagrams in the Green's function of the system are contained by expressing  $w$  as follows

$$w = \text{[diagram of a chain of 10 vertical lines]} + \text{[diagram of a chain of 10 vertical lines connected to a shaded oval labeled } w \text{]} . \quad (23)$$

The corresponding mathematical equations for Eq. 21, 22 and 23 read

$$w_w(11') = v(11') + \int d2d3v(12)\chi_w(23)v(31') \quad (24)$$

$$\chi_e^{(w)}(11') = \chi_e^{(0)}(11') + \iint d2d3 \chi_e^{(0)}(12) w_w(23) \chi_e^{(w)}(31') \quad (25)$$

$$w(11') = w_w(11') + \iint d2d3 w_w(12) \chi_e^{(w)}(23) w_w(31') \quad (26)$$

## 2.3 Special case of the slit geometry

Until now, our work does not depend on the geometry. If the system has one interface, then Eq. 23 can be written in terms of the well-identified response function  $\chi_e^{(w)}$ . In contrast, when two interfaces are present,  $\chi_e^{(w)}$  is the response function for the whole electronic part, that is the two (semi-)metals with a channel filled with water in between. Due to our finite matrix inversion for the liquid part, the finite size channel geometry is necessary and we need to express  $\chi_e^{(w)}$  with the response function of a single graphene sheet  $\chi_e^{(0)}$ .

Naively, we would like to split the electronic response into two parts, one for the electrons at the bottom  $\downarrow$  of the channel and one for the electrons at the top  $\uparrow$  that is

$$\begin{array}{c} \text{[Diagram: Oval with 'W' inside]} \end{array} = \begin{array}{c} \text{[Diagram: Oval with 'W' and two downward arrows inside]} \end{array} + \begin{array}{c} \text{[Diagram: Oval with 'W' and two upward arrows inside]} \end{array}, \quad (27)$$

where the diagrams on the right-hand side are the renormalized response functions for the graphene sheets at  $z = 0$  (bottom,  $\downarrow$ ) and at  $z = L$  (top,  $\uparrow$ ). The diagram on the left-hand side is therefore the first guess. The correct result is not that simple because there are cross correlation effects that have to be considered. Indeed, according to the aforementioned rules, we miss some diagrams in  $w$  and we need to combine top and bottom response functions in all possible ways. We can separate all combination in four categories depending on their first and last diagram ( $\uparrow\uparrow, \uparrow\downarrow, \downarrow\uparrow, \downarrow\downarrow$ ). The task is easier if we introduce the cross correlation response function

$$\begin{array}{c} \text{[Diagram: Oval with 'W' and two upward arrows inside]} \end{array} = \begin{array}{c} \text{[Diagram: Oval with 'W' and two downward arrows inside]} \end{array} \text{---} \begin{array}{c} \text{[Diagram: Oval with 'W' and two upward arrows inside]} \end{array}, \quad (28)$$

and its mean-field renormalized analogue

$$\begin{array}{c} \text{[Diagram: Oval with 'W' and two upward arrows inside]} \end{array} = \begin{array}{c} \text{[Diagram: Oval with 'W' and two downward arrows inside]} \end{array} + \begin{array}{c} \text{[Diagram: Oval with 'W' and two downward arrows inside]} \end{array} \text{---} \begin{array}{c} \text{[Diagram: Oval with 'W' and two downward arrows inside]} \end{array} \quad (29)$$

. This gives the first two independent Dyson equations (Eq. 29 can also be written for  $\uparrow\downarrow$ ) and the remaining two read

$$\begin{array}{c} \text{[Diagram: Oval with 'W' and two downward arrows inside]} \end{array} = \begin{array}{c} \text{[Diagram: Oval with 'W' and two downward arrows inside]} \end{array} + \begin{array}{c} \text{[Diagram: Oval with 'W' and two upward arrows inside]} \end{array} \text{---} \begin{array}{c} \text{[Diagram: Oval with 'W' and two downward arrows inside]} \end{array}, \quad (30)$$

– and the same for  $\uparrow\uparrow$ . Assembling the four categories gives the response function that we look for and

$$\begin{array}{c} \text{[Diagram: Oval with 'W' inside]} \end{array} = \begin{array}{c} \text{[Diagram: Oval with 'W' and two downward arrows inside]} \end{array} + \begin{array}{c} \text{[Diagram: Oval with 'W' and two upward arrows inside]} \end{array} + \begin{array}{c} \text{[Diagram: Oval with 'W' and two downward arrows inside]} \end{array} \text{---} \begin{array}{c} \text{[Diagram: Oval with 'W' and two downward arrows inside]} \end{array} + \begin{array}{c} \text{[Diagram: Oval with 'W' and two upward arrows inside]} \end{array} \text{---} \begin{array}{c} \text{[Diagram: Oval with 'W' and two upward arrows inside]} \end{array}. \quad (31)$$

It can be checked that if the height of the channel tends to infinity, the cross susceptibilities tend to 0 and our initial assumption is correct - i.e. Eq. 31 and Eq. 27 are equal.

## 3 Water model

In this part, we build a versatile model for bulk water that can be adapted to the slab geometry. It relies on the construction of the non-interacting response function  $\chi_w^{(0)}$  and the effective potential between molecules  $v_w^{\text{eff}}$ . We scrutinize the bulk medium before tackling the interface. Then we express the local susceptibility  $\bar{\chi}_w(z)$  in our microscopic description.

### 3.1 Bulk water

#### 3.1.1 Non-interacting susceptibility $\chi_w^{(0)}(k)$

In this paragraph we detail our model for bulk water. First, we precise that we will consider static external perturbations only. The time integration in Eq.1 gives that the mean induced charge density does not depend on



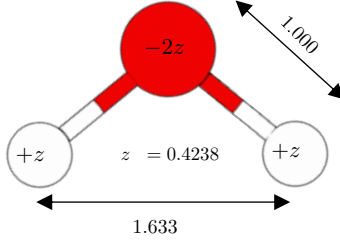


Figure 2: Sketch of a three-point charge SPC/E water molecule. Distances and partial charges are indicated on the figure.

time (as expected) and that the relevant response quantity is the zero-frequency component of the response function - e.g.  $\chi_w(\mathbf{k}) = \chi_w(\mathbf{k}, \omega = 0)$  in the homogeneous and isotropic system. We briefly recall how to obtain it using Kramers-Kronig relationships and the fluctuation-dissipation theorem [Kubo \(1966\)](#) :

$$\chi_w(\mathbf{k}) = \text{Re}\chi_w(\mathbf{k}, \omega = 0) \quad (32)$$

$$\stackrel{\text{KK}}{=} \int_{-\infty}^{+\infty} \frac{d\omega'}{\pi} \frac{\text{Im}\chi_w(\mathbf{k}, \omega')}{\omega'} \quad (33)$$

$$\stackrel{\text{fluc-diss}}{=} \int_{-\infty}^{+\infty} \frac{d\omega'}{\pi} \frac{\omega' - \frac{\omega'}{2k_B T} S_w(\mathbf{k}, \omega')}{\omega'} \quad (34)$$

$$= -\beta S_w(\mathbf{k}, t = 0) = -\beta S_w(\mathbf{k}) \quad (35)$$

$$= -\frac{\beta}{\mathcal{V}} \langle n_w(\mathbf{k}) n_w(-\mathbf{k}) \rangle \quad (36)$$

where  $\langle . \rangle$  means the phase-space averaged at equilibrium,  $S_w(1, 2) = \langle n_w(1) n_w(2) \rangle$  is the charge structure factor,  $\mathcal{V}$  the volume of the system. The charge density of the water molecules  $n_w(\mathbf{x})$  - that must be replaced by  $\delta n_w(\mathbf{x}) = n_w(\mathbf{x}) - \langle n_w(\mathbf{x}) \rangle$  if the mean is not zero - is composed of point-like charges. In a field formulation, we can write the charge density as a convolution between the fixed charge density  $\sigma(\mathbf{x}, \Omega)$  of one rigid water molecule oriented with an angle  $\Omega$ , and the molecular number density  $N_w(\mathbf{x}, \Omega)$  - i.e.  $\int_{\mathcal{V}} \int_{\Omega} N_w = N = n_0 \mathcal{V}$  so that  $n_0$  is the molecular density.

$$N_w(\mathbf{x}, \Omega) = \sum_i \delta(\mathbf{x} - \mathbf{x}_i) \delta(\Omega - \Omega_i) \quad \sigma(\mathbf{x}, \Omega) = \sum_{\alpha} c_{\alpha} \delta(\mathbf{x} - \mathbf{s}_{\alpha}(\Omega)), \quad (37)$$

They both depend on the molecule's orientation  $\Omega$  that we do not need to explicit here, but details can be found in e.g. [Jeanmairet et al. \(2013\)](#). The index  $i$  runs on different molecules and  $\alpha$  on different atoms in the molecule with the partial charges  $c_{\alpha}$ .  $\mathbf{s}_{\alpha}(\Omega)$  is the position of the atom  $\alpha$  given the orientation  $\Omega$  of the molecule. Those quantities for the SPC/E model [Berendsen et al. \(1987\)](#) can be found in Fig. 2. This gives

$$n_w(\mathbf{x}) = \int d\Omega \int d\mathbf{x}' \sigma(\mathbf{x} - \mathbf{x}', \Omega) N_w(\mathbf{x}', \Omega) \quad (38)$$

With those definitions, the structure factor reads

$$S_w(\mathbf{k}) = \frac{1}{\mathcal{V}} \iint d\Omega_1 d\Omega_2 \sigma(\mathbf{k}, \Omega_1) \sigma(-\mathbf{k}, \Omega_2) \langle N_w(\mathbf{k}, \Omega_1) N_w(-\mathbf{k}, \Omega_2) \rangle \quad (39)$$

The molecular number density field can be split into two parts that highlight intramolecular and intermolecular correlations

$$\langle N_w(\mathbf{k}, \Omega_1) N_w(-\mathbf{k}, \Omega_2) \rangle = \langle \sum_i \delta(\Omega_1 - \Omega_i) \delta(\Omega_2 - \Omega_i) \rangle + \sum_{i, j \neq i} \dots \quad (40)$$

Therefore, we can write  $S_w(\mathbf{k}) = S_w^{(0)}(\mathbf{k}) + S_w^{(\text{inter})}(\mathbf{k})$  with

$$S_w^{(0)}(\mathbf{k}) = \frac{1}{V} \int d\Omega_1 \sigma(\mathbf{k}, \Omega_1) \sigma(-\mathbf{k}, \Omega_1) \langle N_w(\Omega_1) \rangle \quad (41)$$

and the orientational density  $N_w(\Omega_1) = \sum_i \delta(\Omega - \Omega_i)$ . In the bulk  $\langle N_w(\Omega_1) \rangle = 1/8\pi^2$  is homogeneous and

$$S_w^{(0)}(\mathbf{k}) = n_0 \sum_{\alpha, \beta} c_\alpha c_\beta \int \frac{d\Omega_1}{8\pi^2} e^{-i\mathbf{k}(\mathbf{s}_\alpha(\Omega_1) - \mathbf{s}_\beta(\Omega_1))} = n_0 \sum_{\alpha, \beta} c_\alpha c_\beta j_0(kd_{\alpha\beta}) \quad (42)$$

where  $j_0$  is the zeroth order spherical Bessel function, the interatomic distances read  $d_{\alpha\beta} = |\mathbf{s}_\alpha - \mathbf{s}_\beta|$  and  $n_0$  is the molecular bulk density. For SPC/E water, we have

$$S_w^{(0)}(k) = n_0 z_H^2 [6 - 8\text{sinc}(kd_{\text{OH}}) + 2\text{sinc}(kd_{\text{HH}})] \quad (43)$$

where  $z_H$  is the partial charge on the hydrogen atom,  $d_{\text{OH}}$  and  $d_{\text{HH}}$  are the bond distances of the SPC/E molecule (see Fig. 2) [Berendsen et al. \(1987\)](#) and  $n_0 = 0.03298 \text{ \AA}^{-3}$ . This gives the response function of the independent - or non-interacting - molecules that reads

$$\chi_w^{(0)}(k) = -\beta S_w^{(0)}(k) \quad (44)$$

### 3.1.2 Effective potential $v_w^{\text{eff}}(k)$

In order to cast the water susceptibility into the mean-field equation [Eq. 10](#), we want to infer the effective inter-molecular potential  $v_w^{\text{eff}}(k)$  such that the equation

$$\chi_w(k) = \chi_w^{(0)}(k) + \chi_w^{(0)}(k) v_w^{\text{eff}}(k) \chi_w(k) \quad (45)$$

is satisfied for the homogeneous, isotropic case. It leads to  $v_w^{\text{eff}}(k) = 1/\chi_w^{(0)}(k) - 1/\chi_w(k)$  as already obtained in [Eq. 19](#). The expression of  $v_w^{\text{eff}}(k)$  is known in the long-wavelength limit as we know that

$$S_w^{(0)}(k) \xrightarrow{k \rightarrow 0} n_0 \frac{4}{3} k^2 z_H^2 d_{\text{OH}}^2 \cos^2\left(\frac{\theta_{\text{HOH}}}{2}\right) = n_0 \frac{k^2 \mu^2}{3} = k_B T n_0 \alpha k^2 \quad (46)$$

where we notice the Debye-Langevin polarizability  $\alpha = \frac{\mu^2}{3k_B T}$  with  $\mu = 2.351 \text{ D}$  the dipole moment of the SPC/E water molecule. Using the dimensionless susceptibility  $\chi_w(k) = -\frac{4\pi\epsilon_0}{1} \frac{k^2}{4\pi} \bar{\chi}_w(k)$  with the limit  $\bar{\chi}_w(k) \xrightarrow{k \rightarrow 0} 1 - \frac{1}{\epsilon_w}$ , we obtain

$$v_w^{\text{eff}}(k) \xrightarrow{k \rightarrow 0} \frac{1}{4\pi\epsilon_0\epsilon_w^{\text{eff}}} \frac{4\pi}{k^2} \quad (47)$$

with the effective dielectric constant given by

$$\frac{1}{\epsilon_w^{\text{eff}}} = \frac{1}{\bar{\chi}_w(k \rightarrow 0)} - \frac{1}{\bar{\chi}_w^{(0)}(k \rightarrow 0)} = 1 + \frac{1}{\epsilon_w - 1} - \frac{\epsilon_0}{n_0 \alpha}. \quad (48)$$

As expected, note that the intermolecular potential is zero — or  $\epsilon_w^{\text{eff}} \rightarrow \infty$  — if water molecules behave independently i.e.  $\bar{\chi}_w \simeq \bar{\chi}_w^{(0)}$ . For water we have  $\epsilon_w^{\text{eff}} \simeq 1.04$  so that the description of interacting molecular form factors with a bare Coulomb potential is quite accurate in the long-wavelength limit. For the remaining wavelengths, with the help of the results from the bulk SPC/E MD [Jeanmairet et al. \(2016\)](#) shown in the main text, we suggest the following ansatz (see main text for formula in reciprocal space):

$$v_w^{\text{eff}}(x) = \frac{1 - e^{-\kappa x} - x\gamma \frac{\kappa}{\pi} e^{-\kappa^2 x^2/2}}{4\pi\epsilon_0\epsilon_w^{\text{eff}} x}. \quad (49)$$

It gives a simple but accurate description of the response function. An inverse screening length  $\kappa$  dictates the position of the overscreening peak and a prefactor  $\gamma \simeq 1$  modifies its amplitude. We have found that  $\kappa = 1.65 \text{ \AA}^{-1}$  and  $\gamma = 0.99$  can reproduce the spectra of SPC/E water. The effect of those parameters on  $\bar{\chi}_w(k)$  is shown in [Fig. 3](#). Note that the experimental spectra [Bopp et al. \(1996\)](#) shows a less intensive peak that can be easily fitted by tuning down  $\gamma$ . The second peak of  $\bar{\chi}_w(k)$  around  $k \simeq 5 \text{ \AA}^{-1}$  can also be included to refine the model, but we expect no important change on the long-range collective dielectric response of water.

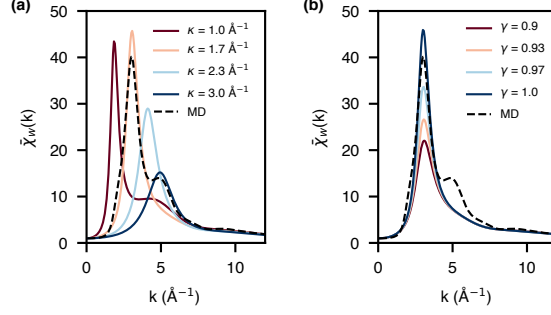


Figure 3: Sensitivity of  $\bar{\chi}_w(k)$  to  $\kappa$  and  $\gamma$  variation. (a) Variation of  $\kappa$  for  $\gamma = 0.99$ . (b) Variation of  $\gamma$  for  $\kappa = 1.65 \text{ \AA}^{-1}$

## 3.2 Interfacial water

### 3.2.1 Non-interacting susceptibility $\chi_w^{(0)}(q, z, z')$

Looking for the response function  $\chi_w(q, z, z')$  at interfaces, we can proceed from Eq. 32 to Eq. 36 to find a relation between the susceptibility and the corresponding structure factor. Equally, we dwell on the non-interacting part and find

$$\chi_w^{(0)}(q, z, z') = -\beta S_w^{(0)}(q, z, z') \quad (50)$$

We proceed like in the bulk and after some straightforward steps, we obtain

$$S_w^{(0)}(\mathbf{q}, z, z') = \frac{1}{\mathcal{A}} \iint d\Omega_1 dz_1 \sigma(\mathbf{q}, z - z_1, \Omega_1) \sigma(-\mathbf{q}, z' - z_1, \Omega_1) \langle N_w(z_1, \Omega_1) \rangle \quad (51)$$

where  $\mathcal{A}$  is the surface area of the interface and

$$\sigma(\mathbf{q}, z, \Omega) = \sum_{\alpha} c_{\alpha} e^{-i\mathbf{q}\mathbf{s}_{\alpha}(\Omega)} \delta(z - z_{\alpha}(\Omega)) \quad N_w(z_1, \Omega) = \sum_i \delta(\Omega_1 - \Omega_i) \delta(z_1 - z_i) \quad (52)$$

Looking at the structure of the product  $\sigma(\mathbf{q}, z, \Omega_1) \sigma(-\mathbf{q}, z', \Omega_1)$ , we can express with the sum and differences of  $z$  and  $z'$  as follows

$$\begin{aligned} \sigma(\mathbf{q}, z, \Omega_1) \sigma(-\mathbf{q}, z', \Omega_1) &= \sum_{\alpha\beta} c_{\alpha} c_{\beta} e^{-i\mathbf{q}(\mathbf{s}_{\alpha}(\Omega) - \mathbf{s}_{\beta}(\Omega))} \delta(z - z_{\alpha}(\Omega)) \delta(z' - z_{\beta}(\Omega)) \\ &= \sum_{\alpha\beta} c_{\alpha} c_{\beta} e^{-i\mathbf{q}(\mathbf{s}_{\alpha}(\Omega) - \mathbf{s}_{\beta}(\Omega))} \delta(z - z' - [z_{\alpha}(\Omega) - z_{\beta}(\Omega)]) \times \delta(z + z' - [z_{\alpha}(\Omega) + z_{\beta}(\Omega)]) \end{aligned} \quad (53)$$

This makes the convolution of Eq. 51 with  $N_w(z_1, \Omega_1)$  possible. It reads

$$S_w^{(0)}(\mathbf{q}, z, z') = \frac{1}{\mathcal{A}} \int d\Omega \sum_{\alpha\beta} c_{\alpha} c_{\beta} e^{-i\mathbf{q}(\mathbf{s}_{\alpha}(\Omega) - \mathbf{s}_{\beta}(\Omega))} \delta(z - z' - [z_{\alpha}(\Omega) - z_{\beta}(\Omega)]) \times N_w\left(\frac{z + z' - [z_{\alpha}(\Omega) + z_{\beta}(\Omega)]}{2}, \Omega\right) \quad (54)$$

For an homogeneous density, we would be able to get the term involving  $N_w$  out of the summation. Assuming equiprobable orientation of molecules in the entire slab, we would recover the inverse Fourier transform of the bulk structure factor, i.e.

$$S_w^{(0)}(\mathbf{q}, |z - z'|) = \int \frac{dq_z}{2\pi} e^{iq_z |z - z'|} S_w^{(0)}(\mathbf{k}) \quad (55)$$

$$= n_0 z_H^2 [6\delta(z - z') - 8I(q, d_{\text{OH}}, |z - z'|) + 2I(q, d_{\text{HH}}, |z - z'|)] \quad (56)$$

with  $I(q, d, z) = J_0(q\sqrt{d^2 - z^2})\Theta(d - |z|)/2d$  and  $J_0$  is the zeroth order Bessel function. We work in this direction and try to express  $S_w^{(0)}(\mathbf{q}, z, z')$  with  $S_w^{(0)}(\mathbf{q}, |z - z'|)$ . Using the condition enforced by the first Dirac delta function in Eq. 54  $-z = z' + [z_\alpha(\Omega) - z_\beta(\Omega)]$  – we can replace the term involving  $N_w$  by either  $N_w(z' - z_\beta(\Omega), \Omega)$ , or  $N_w(z - z_\alpha(\Omega), \Omega)$ , but also by  $\sqrt{N_w(z - z_\alpha(\Omega), \Omega) N_w(z' - z_\beta(\Omega), \Omega)}$ , without any approximation. Making now the approximation  $N_w(z - z_\alpha, \Omega) \simeq N_w(z, \Omega)$  and assuming equiprobable orientation of molecules in the entire slab we can write

$$S_w^{(0)}(q, z, z') \simeq \frac{\sqrt{n_0(z)n_0(z')}}{n_0} S_w^{(0)}(q, |z - z'|), \quad (57)$$

which is the main result of this paragraph. This approximation is valid if the molecular profile typically varies on a scale larger than the size of a water molecule. Note however that the Taylor expansion of  $N_w$  near the interface give rises to terms linear in  $z_\alpha(\Omega)$  that can most probably gives a zero contribution when the angular integration is carried out (under the approximation of equiprobable orientation). Combining Eq. ?? and Eq. 57 gives the equation (Eq. 4) of the main text.

### 3.2.2 Effective potential $v_w^{\text{eff}}(q, |z - z'|)$

What is the charge-charge effective potential in the water slab ? We don't know it, but we can suppose that *water molecules interact in the slab as if they were in the bulk*. This is a common approximation in the liquid state theories of water - e.g. Jeanmairet *et al.* (2013). We therefore take  $v_w^{\text{eff}}$  from Eq. 49 and give for completeness the appropriate Fourier transform that reads

$$v_w^{\text{eff}}(q, |z - z'|) = \frac{1}{4\pi\epsilon_0\epsilon_w^{\text{eff}}} \left( \frac{2\pi}{q} e^{-q|z-z'|} - \frac{2\pi}{Q} e^{-Q|z-z'|} - \gamma \frac{2\pi}{\kappa} e^{-q^2/2\kappa^2} \frac{e^{-\kappa^2(z-z')^2}}{\pi} \right), \quad (58)$$

where  $Q^2 = q^2 + \kappa^2$ . Those expressions are all linked by Fourier transform.

### 3.2.3 Matrix filling

The matrix  $X_w^{(0)}$  has a size  $\lfloor L/dz \rfloor \times \lfloor L/dz \rfloor$  with grid spacing  $dz = 0.02\text{\AA}$  and length  $L = 6\text{nm}$ . We rely on the condition that an homogeneous external potential cannot induce a charge density disturbance (i.e.  $\int dz' \chi_w^{(0)}(z, z') = 0$ ) to fill the matrix. This can be checked in the bulk and imposed at altitudes close to the molecular density depletion. Therefore, in order to obtain the entire matrix  $X_w^{(0)}$  and avoid numerical integration errors due to the Dirac delta functions, we fill the non-diagonal entries of  $X_w^{(0)}$  according to  $\chi_w^{(0)}(q, z, z') = -\beta S_w^{(0)}(q, z, z')$  and impose that all lines and column sum to 0 to fill the diagonal.

## 4 Local dielectric susceptibility $\bar{\chi}_w(z)$

### 4.1 Expression from $\chi_w(q, z, z')$

In order to confirm our model for water, we define the following non-local dielectric function

$$\varepsilon_w^{-1}(q, z, z') = \delta(z - z') + \int dz_1 v(q, z, z_1) \chi_w(q, z_1, z') \quad (59)$$

with the converged grid spacing  $dz = 0.02\text{\AA}$ . The expression for the kernel  $\varepsilon_w^{-1}(r, r')$  is derived from the bulk relation between  $\langle \phi_{\text{tot}} \rangle$  and  $\phi_{\text{ext}}$ ,

$$\langle \phi_{\text{tot}} \rangle(r) = \phi_{\text{ext}}(r) + \int d^3r'' d^3r' v(r, r'') \chi_w(r'', r') \phi_{\text{ext}}(r') \quad (60)$$

that we obtained using Eqs. (4,5)

At this point, we still have a function of three variables that we cannot easily visualize. We therefore want to link  $\varepsilon_w^{-1}(q, z, z')$  to the inverse local dielectric function  $\varepsilon_w^{-1}(z)$  that relates the total electric field  $E_z(z)$  in the system to the constant one that is applied. Again, instead of turning back to electrostatics, we construct microscopically the external electric field. We place two infinite plates of opposite surface charge that sandwich from very far the system under scrutiny. The external electric field in the system is constant and equal to  $D_z/\epsilon_0$ . Seen by the system



of finite size under scrutiny, this homogeneous (in the plane), constant displacement field applied in the direction normal to the surface can be written as  $\phi_{\text{ext}}(z) = -\frac{D_z}{\epsilon_0}z$  plus a constant that we set to zero. The electric field in the system reads  $\partial_z \phi_{\text{tot}}(z) = -E_z(z)$ . Also, for the microscopic linear response framework that we use, the electrostatic potentials are linked as follows :

$$\phi_{\text{tot}}(z) = \int_0^L \epsilon_w^{-1}(q \rightarrow 0, z, z') \phi_{\text{ext}}(z') dz' \quad (61)$$

The electric field and the constant displacement field are linked via the local dielectric function such that

$$E_z(z) = \epsilon_0^{-1} \epsilon_w^{-1}(z) D_z \quad (62)$$

We can differentiate Eq. 61 and use Eq. 62 to obtain

$$\epsilon_w^{-1}(z) = \partial_z \int_0^L dz' \epsilon_w^{-1}(q \rightarrow 0, z, z') z' \quad (63)$$

from which the local susceptibility reads  $\bar{\chi}_w(z) = 1 - \epsilon_w^{-1}(z)$ . It relates the polarization of the medium to the applied electric field  $\epsilon_0 E_z(z) = D_z - P_z(z)$  where  $P_z(z) = \bar{\chi}(z) D_z$ .

## 4.2 Comparison with Landau-Ginzburg model

The smoothed step function molecular density profile  $n_0(z)$  is chosen because:

- the use of  $v_w^{\text{eff}}$  that implies that molecules interact as is they were in the bulk, that is with an homogeneous molecular density  $n_0$ .
- it gives the same  $\bar{\chi}_w(z)$  we obtain by using the real hydrogen density from the MD simulation. We use the hydrogen atoms because they can go at lower altitudes than the oxygen atoms.

Its expression is given by

$$n_0(z) = \frac{n_0}{4} \left[ \tanh\left(\frac{z - d_0}{\sigma_0}\right) + 1 \right] \left[ \tanh\left(\frac{L - z - d_0}{\sigma_0}\right) + 1 \right].$$

We can see the effect of the smoothness in Fig. 4a. The agreement with the Landau-Ginzburg model introduced in (Monet *et al.*, 2021) is excellent for  $\sigma_0 = 0.2\text{\AA}$ . Compared to the MD results (Monet *et al.*, 2021) in Fig. 4b, the use of  $\sigma_0 = 0.3\text{\AA}$  gives the correct amplitude for the first peak. The oscillation period, amplitude and decay length are also in good agreement. By tuning the molecular density profile, we can fit exactly the MD profile, but our goal is not to reproduce the local dielectric of an MD simulation that uses effective Lennard-Jones potentials or effective interactions between the surface and the water molecules – graphene must be absent when we build  $\chi_w$ .

## 5 Graphene model

Here we give the expression for the non-interacting and the interacting response function of graphene.

### 5.1 The non-interacting susceptibility $\chi_e^{(0)}(q, z, z')$

The non-interacting response function of graphene sheet  $\chi_e^{(0)}(q)$  can be calculated with a tight-binding model at  $T = 0\text{K}$  Hwang and Das Sarma (2007). It reads

$$\chi_e^{(0)}(q) = -\frac{2k_F}{\hbar v_F \pi} \left[ 1 + \frac{1}{2} \Theta\left(\frac{q}{2k_F} - 1\right) \left( \frac{\pi}{2} \frac{q}{2k_F} - \sqrt{1 - \left(\frac{2k_F}{q}\right)^2} - \frac{q}{2k_F} \arcsin\left(\frac{2k_F}{q}\right) \right) \right]$$

where  $v_F = 1 \text{ nm.fs}^{-1}$  is the Fermi velocity and  $k_F = E_F/\hbar v_F$  is the Fermi wave vector and  $E_F$  the Fermi energy. The effect of temperature and Fermi level  $E_F$  is not investigated in this article and we rather use a minimal Fermi level doping  $E_F = k_B T$  that represents the minimal concentration of mobile electrons.

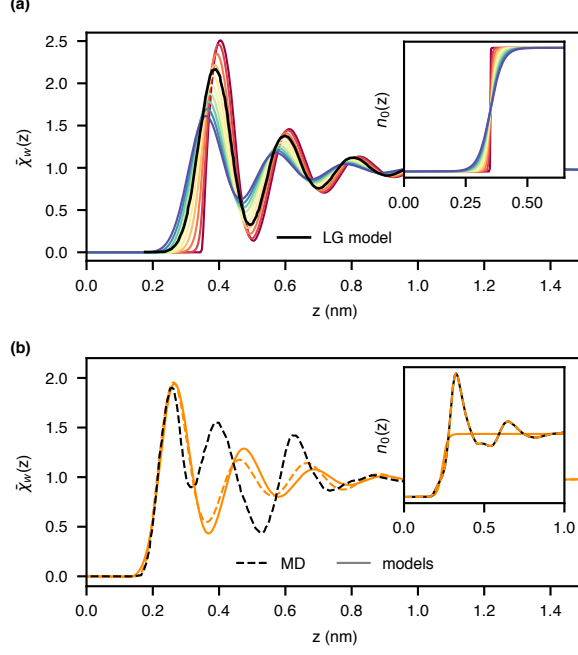


Figure 4: **(a)** Local dielectric susceptibility of the slab  $P_z = \bar{\chi}_w(z)D_z$  computed from the non-local response function  $\chi_w(q, z, z')$  with varying smoothness of the step function  $\sigma$  and compared with Landau-Ginzburg model of Ref. (Monet *et al.*, 2021). **(b)** Models of the main text compared with the results from the MD simulation of (Monet *et al.*, 2021). The force field parameters chosen for water and graphene are taken from Ref. (Werder *et al.*, 2003).

## 5.2 The interacting susceptibility $\chi_e^{(w)}(q, z, z')$

For two confining plates centered in  $z = 0$  and  $z = L$ , the expression of the electronic response function is obtained by following the steps from Eq. 27 to Eq. 31. This gives

$$\chi_e^{(w)}(q, z, z') = \chi_{e\uparrow}^{(w)}(q)\delta(z)\delta(z') + \chi_{e\downarrow}^{(w)}(q)\delta(L-z)\delta(L-z') + \chi_{e\uparrow\downarrow}^{(w)}(q)\delta(z-L)\delta(z') + \chi_{e\downarrow\uparrow}^{(w)}(q)\delta(z)\delta(L-z') \quad (64)$$

with

$$\chi_{e\uparrow}^{(w)}(q) = \frac{\chi_{e/Gr}^{(w)}(q)}{1 - [w_w(q, 0, L)\chi_{e/Gr}^{(w)}(q)]^2} \quad \chi_{e\downarrow}^{(w)}(q) = \chi_{e\uparrow}^{(w)}(q) \quad (65)$$

$$\chi_{e\uparrow\downarrow}^{(w)}(q) = \frac{\chi_{e/Gr}^{(w)}(q)w_w(q, 0, L)\chi_{e/Gr}^{(w)}(q)}{1 - [w_w(q, 0, L)\chi_{e/Gr}^{(w)}(q)]^2} \quad \chi_{e\downarrow\uparrow}^{(w)}(q) = \chi_{e\uparrow\downarrow}^{(w)}(q) \quad (66)$$

and where

$$\chi_{e/Gr}^{(w)}(q) = \frac{\chi_e^{(0)}(q)}{1 - w_w(q, 0, 0)\chi_e^{(0)}(q)} \quad (67)$$

The “uncoupled” and “semi-coupled” curves in the main text are obtained by replacing  $w_w(q, 0, 0)$  with  $v(q, 0, 0) = \frac{1}{4\pi\epsilon_0} \frac{2\pi}{q}$  in Eq. 67.

## 6 Supplementary discussions

### 6.1 Long-wavelength limit error for water

In the case of the infinite height channel  $L \rightarrow \infty$ , Eq. 64 reduces to  $\chi_e^{(w)}(q, z, z') = \chi_{e/\text{Gr}}^{(w)}\delta(z)\delta(z')$  such that the system's Green's function reads

$$w(q, z, z') = w_w(q, z, z') + w_w(q, z, 0)\chi_e^{(w)}(q)w_w(q, 0, z'). \quad (68)$$

Close to the surface, for  $z \simeq z' \simeq 0$ , if we take the long-wavelength limit according Eq. 72, the second on the rhs of Eq. 68 is reduced by a factor a roughly  $(\epsilon_w^*)^2 \simeq 1600$  for water, as first stated in Kornyshev and Vorotyntsev (1980).

### 6.2 Comparison with other studies considering a metallic behavior of the surface

To evaluate the role of the graphene sheet, we can isolate the electronic part  $F_e = F - F_w$ , where  $F_w$  solely contains the contribution of water and is obtained via the equation (Eq. 7) of the main text, replacing  $w$  by  $w_w$ . The details of the contributions are shown in Fig. 5. Note that the blue curve 'water only' corresponds to  $\Delta F$  as defined in Eq. (7) and is represented to permit an estimation of the electronic stabilization amplitude. In this case, the electronic contribution vanishes. We report on the same figure the results of Ref. (Misra and Blankstein, 2021) that decomposes the wall-ion contribution for the adsorption site of  $\text{SCN}^-$ , which is an ion too large and anisotropic to be quantitatively compared with isotropic ion in presence of water. Nevertheless, the good agreement with our results regarding metal-ion potential attenuation validates our description of the system.

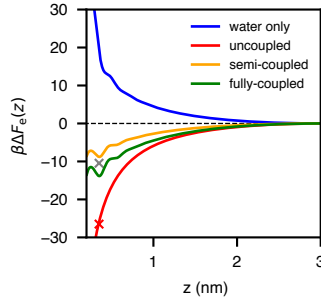


Figure 5: Details of the contribution of the PMF shown in the main text. The crosses are results extracted from Ref. (Misra and Blankstein, 2021).

Note that it is not possible to disentangle electronic and water contribution of the PMF when metallic character of the graphene surface is neglected, which is the case in classical MD simulations.

### 6.3 Electron-electron potential attenuation

For an infinite channel height  $L \rightarrow \infty$ , we have

$$w_w(q, 0, 0) = \frac{1}{4\pi\epsilon_0} \frac{2\pi}{q} [1 - g_w(q)], \quad (69)$$

where  $g_w(q)$  is the surface response function of the water medium, defined as

$$g_w(q) = -\frac{1}{4\pi\epsilon_0} \frac{2\pi}{q} \iint_0^{+\infty} dz dz' e^{-q(z+z')} \chi_w(q, z, z'), \quad (70)$$

and that converges to the image charge coefficient in the long-wavelength limit Kavokine *et al.* (2022)

$$g_w(q) \xrightarrow{q \rightarrow 0} \frac{\epsilon_w - 1}{\epsilon_w + 1}. \quad (71)$$

This gives a two-dimensional screening potential reduced by a factor  $\varepsilon_w^* = (\varepsilon_w + 1)/2$  such that

$$w_w(q, 0, 0) \xrightarrow{q \rightarrow 0} \frac{1}{4\pi\epsilon_0\varepsilon_w^*} \frac{2\pi}{q}. \quad (72)$$

This is the potential by which electrons interact in graphene.

## References

- J. Schwinger, in *Classical Electrodynamics* (Westview Press, 1998).
- G. D. Mahan, *Many-Particle Physics* (Springer US, 1990).
- J.-P. Hansen and I. R. McDonald, *Theory of simple liquids* (Academic Press, 2013).
- D. Bohm and D. Pines, *Physical Review* **92**, 609 (1953).
- N. Kavokine, M.-L. Bocquet, and L. Bocquet, *Nature* **602**, 84 (2022).
- L. Hedin and S. Lundqvist, *Solid State Physics* **23**, 1 (1970).
- F. Giustino, *Reviews of Modern Physics* **89**, 015003 (2017).
- R. Kubo, *Rep. Prog. Phys.* **29** (1966).
- G. Jeanmairet, M. Levesque, R. Vuilleumier, and D. Borgis, *J. Phys. Chem. Lett.* , 6 (2013).
- H. J. C. Berendsen, J. R. Grigera, and T. P. Straatsma, *The Journal of Physical Chemistry* **91**, 6269 (1987).
- G. Jeanmairet, N. Levy, M. Levesque, and D. Borgis, *Journal of Physics: Condensed Matter* **28**, 244005 (2016).
- P. A. Bopp, A. A. Kornyshev, and G. Sutmann, *Physical Review Letters* **76**, 1280 (1996).
- G. Monet, F. Bresme, A. Kornyshev, and H. Berthoumieux, *Physical Review Letters* **126**, 216001 (2021).
- T. Werder, J. H. Walther, R. L. Jaffe, T. Halicioglu, and P. Koumoutsakos, *The Journal of Physical Chemistry B* **107**, 1345 (2003).
- E. H. Hwang and S. Das Sarma, *Physical Review B* **75**, 205418 (2007).
- A. A. Kornyshev and M. A. Vorotyntsev, *Surface Science* **101**, 23 (1980).
- R. P. Misra and D. Blankschtein, *The Journal of Physical Chemistry C* **125**, 2666 (2021).